

Structural and Mechanistic Insights into STIM1-Mediated Initiation of Store-Operated Calcium Entry

Peter B. Stathopoulos,¹ Le Zheng,¹ Guang-Yao Li,¹ Michael J. Plevin,¹ and Mitsuhiro Ikura^{1,*}

¹Division of Signaling Biology, Ontario Cancer Institute and Department of Medical Biophysics, University of Toronto, Toronto Medical Discovery Tower, MaRS Centre, 101 College Street, Toronto, Ontario M5G 1L7, Canada

*Correspondence: mikura@uhnres.utoronto.ca

DOI 10.1016/j.cell.2008.08.006

SUMMARY

Stromal interaction molecule-1 (STIM1) activates store-operated Ca^{2+} entry (SOCE) in response to diminished luminal Ca^{2+} levels. Here, we present the atomic structure of the Ca^{2+} -sensing region of STIM1 consisting of the EF-hand and sterile α motif (SAM) domains (EF-SAM). The canonical EF-hand is paired with a previously unidentified EF-hand. Together, the EF-hand pair mediates mutually indispensable hydrophobic interactions between the EF-hand and SAM domains. Structurally critical mutations in the canonical EF-hand, “hidden” EF-hand, or SAM domain disrupt Ca^{2+} sensitivity in oligomerization via destabilization of the entire EF-SAM entity. In mammalian cells, EF-SAM destabilization mutations within full-length STIM1 induce punctae formation and activate SOCE independent of luminal Ca^{2+} . We provide atomic resolution insight into the molecular basis for STIM1-mediated SOCE initiation and show that the folded/unfolded state of the Ca^{2+} -sensing region of STIM is crucial to SOCE regulation.

INTRODUCTION

Spatiotemporal cytoplasmic Ca^{2+} oscillations differentially regulate myriad processes including apoptosis, contraction, exocytosis, fertilization, immunity, proliferation, and transcription (Berridge et al., 2003). The link between inositol 1,4,5-triphosphate-mediated depletion of endoplasmic reticulum (ER) luminal Ca^{2+} and the activation of Ca^{2+} -permeable, store-operated Ca^{2+} (SOC) channels on the plasma membrane (PM) is termed store-operated Ca^{2+} entry (SOCE) and is a major Ca^{2+} entry pathway in electrochemically nonexcitable cells, providing a sustained cytoplasmic Ca^{2+} influx from the extracellular space (Putney, 1986). SOCE is evolutionarily conserved from roundworms to mammals, implying a fundamental disposition of this process to eukaryotes. In T cells and other lymphocytes, SOCE through Ca^{2+} release-activated Ca^{2+} (CRAC) channels provides the principal source of cytoplasmic Ca^{2+} that signals cytokine secretion and proliferation crucial to the immune response (Feske, 2007).

Genetically impaired CRAC channels in severe combined immunodeficiency disease (SCID) patients lead to dysfunctional T and B cell activation and proliferation (Feske et al., 2006).

STIM1 is a single-pass, type-I transmembrane protein of 685 amino acids and is the ER-resident protein established as the SOCE activator in response to depletion of luminal Ca^{2+} (Liou et al., 2005; Roos et al., 2005; Zhang et al., 2005). The luminal N-terminal region of STIM1 includes an ER signal peptide, an EF-hand domain, and a SAM domain, whereas the cytosolic portion consists of two coiled-coil domains, a Pro/Ser-rich region, and a Lys-rich region (Figure 1A) (Manji et al., 2000; Williams et al., 2001, 2002). Luminal Ca^{2+} depletion results in redistribution of STIM1 from ER homogeneity to punctae in close apposition to the PM; punctae formation precedes SOC influx, implying a causal role for STIM1 aggregation in SOCE activation (Liou et al., 2005; Luik et al., 2006; Wu et al., 2006; Zhang et al., 2005). The EF-hand and SAM domains (EF-SAM) are vital to SOCE regulation, as Ca^{2+} -binding mutants form punctae and activate SOCE independent of Ca^{2+} (Liou et al., 2005; Mercer et al., 2006; Soboloff et al., 2006b; Zhang et al., 2005) and SAM deletion mutants lack the ability to form inducible punctae (Baba et al., 2006). Recombinant EF-SAM alone is capable of oligomerization via Ca^{2+} -depletion-induced structural changes, coupling N-terminal Ca^{2+} sensing with SOCE initiation (Stathopoulos et al., 2006). The cytosolic C-terminal portion is essential for the redistribution of STIM1 oligomers to ER-PM junctions and subsequent SOC channel opening (Baba et al., 2006; Huang et al., 2006; Liou et al., 2007). STIM2 is a mammalian homolog that deviates from STIM1 in sequence similarity proximal to the coiled-coil domains toward the C terminus (Soboloff et al., 2006a; Williams et al., 2001).

Pedigree analysis of inheritable SCID and interfering ribonucleic acid (RNA) experiments identified Orai1 as another major SOC/CRAC channel regulator (Feske et al., 2006; Vig et al., 2006b; Zhang et al., 2006), later confirmed as a subunit of the PM pore (Prakriya et al., 2006; Vig et al., 2006a; Yeromin et al., 2006). Coexpression of STIM1 and Orai1 results in substantial potentiation of SOCE in cultured cells (Mercer et al., 2006; Peinelt et al., 2006; Soboloff et al., 2006b). This dramatic synergism suggests that STIM1 and Orai1 constitute the principal molecular machinery involved in SOCE; the former component serves as the ER Ca^{2+} sensor and activator of SOC/CRAC channels, and the latter serves as the Ca^{2+} -selective channel on the PM.

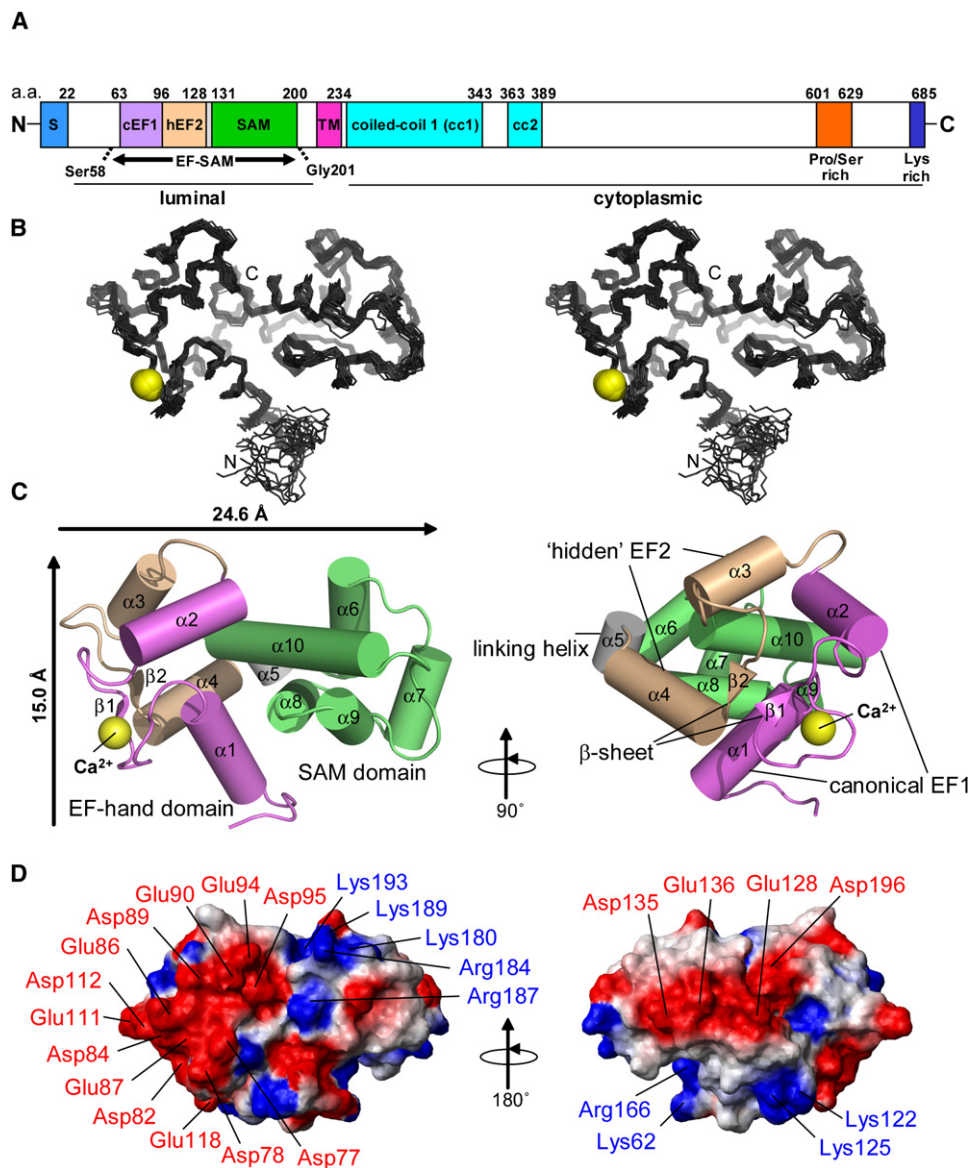


Figure 1. STIM1 Contains a “Hidden” EF-hand

(A) Domain architecture of human STIM1. Sequence analysis identifies a single canonical EF-hand (cEF1; violet); however, the 3D structure reveals a second, “hidden” EF-hand (hEF2; beige) and a short linker helix (gray) between hEF2 and the sterile α motif domain (SAM; green). S, ER signal peptide (blue); TM, transmembrane region (magenta); cc1, coiled-coil domain 1 (cyan); cc2, coiled-coil domain 2 (cyan). Amino and carboxy termini are denoted by N and C, respectively. The amino acid number (aa) is indicated at the top of the figure, and the cellular compartment is indicated at the bottom. We note the suggestion of a vestigial EF-hand in STIM proteins (Hogan and Rao, 2007).

(B) Stereo backbone view of the 20 lowest-energy EF-SAM structures. The yellow spheres represent Ca^{2+} in cEF1.

(C) Secondary structure components of EF-SAM. The structural topology includes $\alpha 1$ (residues 64–73), $\beta 1$ (82–83), $\alpha 2$ (89–97), $\alpha 3$ (102–108), $\beta 2$ (115–116), $\alpha 4$ (117–126), $\alpha 5$ (128–131), $\alpha 6$ (134–145), $\alpha 7$ (150–157), $\alpha 8$ (161–168), $\alpha 9$ (171–174), $\alpha 10$ (183–199). Cylinders are α helices (ten in total) and arrowheads are β strands (two in total, making up one sheet). Motif coloring is consistent with (A).

(D) Electrostatic surface potential of EF-SAM. Basic charges are shown in blue, and acidic charges are shown in red. Residues forming prominent charged patches are indicated.

Despite progress in identifying the SOCE machinery, structural understanding of this process at the atomic level was lacking. Here, we employed NMR spectroscopy and other structural and functional approaches to elucidate the basis for STIM1 Ca^{2+} sensing in the ER with respect to SOCE.

RESULTS

NMR Structure of the Ca^{2+} -Loaded EF-SAM Domain

Several N-terminal STIM1 constructs were engineered (residues 1–201, 23–213, 58–201, 58–128, 110–201, 115–201, and

125–201) as structural targets. Since STIM1 N-terminal sequence alignments indicate that the EF-hand and SAM domains are the only conserved domains from worms to flies to humans (Strange et al., 2007) and 58–201 demonstrated the highest fraction of secondary structure on a per residue basis (far-UV circular dichroism [CD]), we pursued structural studies using this minimally bounded construct representative of all STIM proteins. Recombinant human STIM1 EF-SAM (Ser58 to Gly201) exhibits a well-dispersed ^1H - ^{15}N HSQC spectrum in the presence of Ca^{2+} (Figure S1A, see Supplemental Data available online). Consequently, we implemented conventional heteronuclear NMR spectroscopy (Kanelis et al., 2001) to determine the three-dimensional (3D) structure of this luminal region of STIM1. The 20 lowest-energy structures presented in the stereo ensemble have a post-water refinement backbone root-mean-square deviation (rmsd) of $0.49 \pm 0.07 \text{ \AA}$ (Figure 1B). The structural statistics for the ensemble are given in Table S1. At the structural level, the EF-hand and SAM domains are organized into a single, predominantly α -helical, cooperative and compact globular fold (Figure 1C).

The canonical Ca^{2+} -binding EF-hand (cEF1) forms a conventional helix-loop-helix EF motif ($\alpha 1\beta 1\alpha 2$) (Kretsinger and Nockolds, 1973). This EF-hand motif was previously thought to be the stand-alone functional unit responsible for Ca^{2+} binding in STIM proteins (Baba et al., 2006; Cai, 2007; Liou et al., 2005; Mercer et al., 2006; Roos et al., 2005; Soboloff et al., 2006b; Williams et al., 2001; Zhang et al., 2005). However, our structure shows that EF-SAM contains a second EF-hand ($\alpha 3\beta 2\alpha 4$). This “hidden” EF-hand (hEF2) stabilizes the canonical EF-hand through hydrogen bonding between respective loop regions of each motif (C(O) Val83, Ile115: N(H) Val83, Ile115), forming a small antiparallel β sheet (Figure S1B) as identified in other canonical EF-hand pairs (Ikura et al., 1985). A short helix ($\alpha 5$) links the EF-hand domain with the SAM domain that folds into the well-characterized 5-helix bundle (Stapleton et al., 1999; Thanos et al., 1999) consisting of helices $\alpha 6$ – $\alpha 10$ (Figure 1C). The sequence similarity between STIM1 and STIM2 (58% identity and 88% similarity for EF-SAM) predicts a similar structure for STIM2 EF-SAM.

A structural comparison using Dali found no EF-hand and SAM domain associations in the Protein Data Bank (PDB). The STIM1 EF-hand pair best matches the C-terminal domain of bovine Ca^{2+} -calmodulin (C-CaM) (Dali Z = 2.1, rmsd = 3.2 \AA) (Figure S2A). Vector-geometry mapping of C-CaM and the EF-hand domain of STIM1 shows that each EF-hand motif is in the “open” conformation (interhelical angles of 80.0° versus 81.4° for EF-hand 1; 96.7° versus 107.7° for EF-hand 2, respectively) (Figure S2B; Table S2). The paired EF-hands in EF-SAM intimately interact with the SAM domain; the hydrophobic surface of the “open” EF-hands is buried against nonpolar SAM contacts (see below). The STIM1 SAM domain most resembles SAM of the EphB2 receptor (Dali Z = 4.0, rmsd = 2.1 \AA) (Figure S2C). A structure-based sequence alignment of several SAM domains with STIM1 demonstrates the conservation of primarily hydrophobic residues within each helix (Figure S3). Additionally, the acidic residues in $\alpha 7$ and the basic residues in $\alpha 10$ of STIM1 are conserved through all SAM structures aligned. The present EF-SAM structure exhibits a rare example of an extracel-

lular SAM domain, as a small fraction of STIM1 exists on the PM (Kim and Bowie, 2003; Manji et al., 2000).

The electrostatic surface of EF-SAM is primarily negative at neutral pH (Figure 1D). Two prominent acidic clusters are apparent from the surface charges. Several residues from cEF1 and hEF2 form a highly concentrated negative patch proximate to the Ca^{2+} -liganding site (cEF1: Asp77, Asp78, Asp82, Asp84, Glu86, Glu87, Asp89, Glu90, Glu94, Asp95; hEF2: Glu111, Asp112, Glu118). The second negative region is formed on the opposite side of the protein with anionic charge contributions from hEF2 and the SAM domain (hEF2: Glu128; SAM: Asp135, Glu136, Asp196). It is noteworthy that whereas the EF-hand domain is chiefly acidic, the largest positive cluster of amino acids ($\alpha 10$: Lys180, Arg184, Arg187, Lys189, Lys193) is located on the SAM domain. The precise significance of these charged surfaces is unknown; however, they may afford binding sites for other ER proteins, nucleic acids, or membrane lipids.

EF-Hand and SAM Domain Interactions

The EF and SAM domains of STIM1 fold cooperatively, and folding is well approximated by two-state thermodynamics (Stathopoulos et al., 2006). Recombinant expression of cEF1 and hEF2 results in a constitutively ($\pm \text{Ca}^{2+}$) unfolded protein, as evidenced by far-UV CD (data not shown). Expression of SAM alone yields little or no protein. The separate instability of the EF-hand and SAM domains is consistent with the two-state folding equilibrium of the EF-SAM entity, in which the domains do not fold discretely, but are dependent on each other for concerted folding. This mutual folding cooperativity is not surprising, as the structure reveals robust contacts between these domains. The interaction between the EF and SAM domains is chiefly hydrophobic in nature. At least 11 amino acids from cEF1 and hEF2 form a well-defined hydrophobic cleft (Figure 2A). Leu195 and Leu199 on helix $\alpha 10$, proximal to the C terminus of SAM, provide prominent anchor residues for the cleft, restraining EF-SAM as a single structural entity (Figures 2B, 2C, and S1B). The minimal variation in both the cleft and the anchor nonpolar side chains within the 20-structure ensemble attest to the compact core formed by these residues (Figure 2D). The orientation of the anchoring residues in $\alpha 10$ (Leu195 and Leu199) of the SAM domain with respect to cEF1 and hEF2 (Figure 2C) is akin to the anchoring peptide residues of smMLCK (Leu813) and other kinases with respect to CaM EF helices (Figure S2D) (Chin and Means, 2000; Ikura et al., 1992; Meador et al., 1993). A minor distinction is the rotation ($\sim 30^\circ$) of the STIM1 EF-hand domain about the anchoring residue protrusion compared to Ca^{2+} -CaM:kinase peptide complexes. Internal association of the STIM1 EF-hand hydrophobic cleft with the SAM domain through a CaM-target recognition-like interaction precludes nonspecific associations via this sticky cleft and curtails destabilizing solvent exposure of hydrophobic residues in both domains.

Mutational Analysis of EF-SAM Oligomerization Function

Since STIM1 oligomerization is the molecular trigger for SOCE activation in response to diminished luminal Ca^{2+} (Liou et al., 2007), it is important to dissect out specific interactions critical for the initiation of this process. Mutations were engineered in

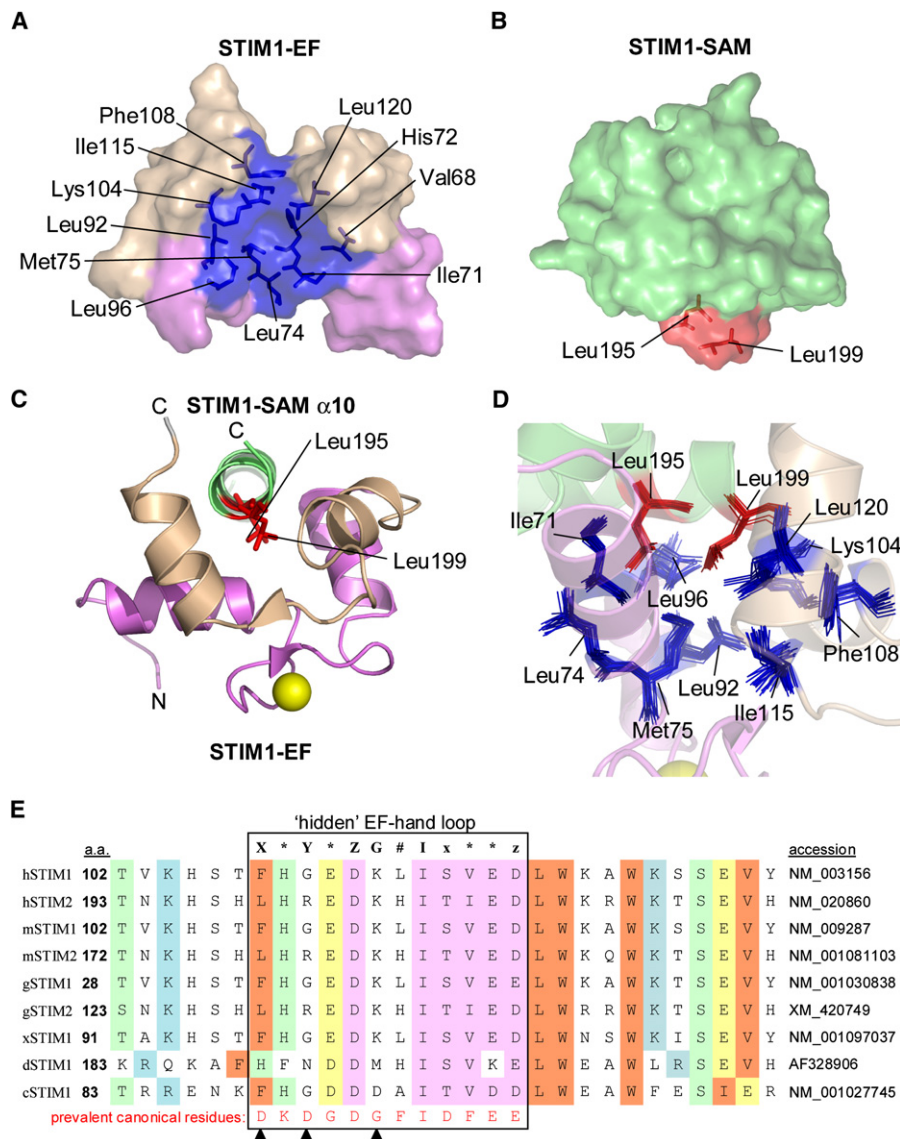


Figure 2. EF-Hand Interactions with SAM Are Mediated by Hydrophobics

(A) Surface representation of the hydrophobic cleft formed by cEF1 and hEF2. Channel-forming residues are indicated as blue sticks.

(B) Surface representation of the hydrophobic protrusion formed by SAM. The anchoring residues are shown as red sticks.

(C) Ribbon diagram of the EF-hand recognition mechanism of SAM. The anchoring residues on α 10 of SAM (red sticks) are directed toward the "open" EF-hands. (D) Specific EF-hand:SAM hydrophobic interactions. Side chains (sticks) from the 20 lowest-energy structures are overlaid, showing a relatively immobile EF-hand:SAM interaction. (z rotated \sim 90° relative to [A]).

(E) "Hidden" EF-hand sequence alignments. Conserved hydrophobic residues are shaded orange, basic residues are shaded blue, acidic residues are shaded yellow, and all other residue conservation is shaded green. Within the Ca^{2+} -binding loop, residues that occur with >10% frequency in a survey of 165 Ca^{2+} -binding EF-hands are shaded magenta (Marsden et al., 1990). The most prevalent residue type in Ca^{2+} -binding EF-hand loops are shown in red. Asp, Ser, and Thr occur with frequencies of 33%, 19%, and 11%, respectively, at position "x." Mutagenesis sites aimed at mobilization of Ca^{2+} binding in hEF2 are indicated with black triangles. h, *Homo sapiens*; g, *Gallus gallus*; m, *Mus musculus*; x, *Xenopus laevis*; d, *Drosophila melanogaster*; c, *Caenorhabditis elegans*. Motif coloring is consistent with Figure 1A. Yellow spheres represent Ca^{2+} .

each motif to elucidate potential modes of EF-SAM interaction (Figures 3A and 3B). The quaternary structure of EF-SAM was assessed by using size-exclusion chromatography (SEC) and multiangle light scattering (MALS). Wild-type EF-SAM exists as a monomer (mass = 17.4 kDa) in the presence of Ca^{2+} , but it elutes as a dimer and oligomer in the absence of Ca^{2+} (Figures

3C and 3E; Table 1). Previously identified Ca^{2+} -binding mutations in cEF1 (Glu87Ala or Asp76Ala) that form punctae constitutively (Liou et al., 2005; Mercer et al., 2006; Soboloff et al., 2006b; Zhang et al., 2005) also form persistent EF-SAM aggregates in our assay (Table 1). The Pro101Gly mutation located in the loop linking cEF1 and hEF2 (Figure 3B) does not affect the

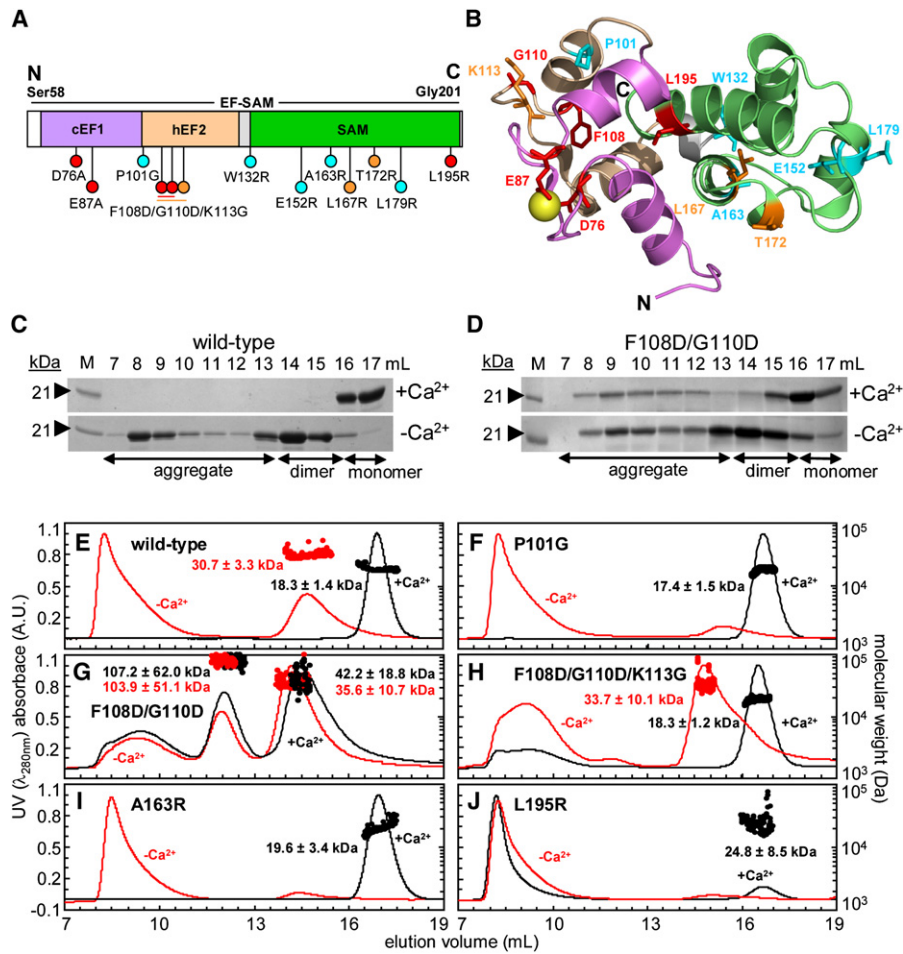


Figure 3. EF-SAM Stability Is Linked to Aggregation Propensity

(A) EF-SAM mutants engineered relative to sequence space. Red mutations cause constitutive EF-SAM aggregation (\pm Ca²⁺) and were engineered into full-length STIM1 for in-cell studies. Orange mutants also result in persistent EF-SAM aggregation. Cyan mutants behave as wild-type.

(B) EF-SAM mutants relative to the 3D structure. Side chains shown as sticks are colored as per (A). Motif coloring is consistent with Figure 1A. The yellow sphere is Ca²⁺.

(C and D) SDS-PAGE of trichloroacetic acid (TCA)-concentrated size-exclusion chromatography elution fractions (\pm Ca²⁺). Elution volume is shown at the top of the figure, marker molecular weight is shown at the left, and solution condition is shown at the right, where +Ca²⁺ = 2.5 mM CaCl₂ and -Ca²⁺ = 5 mM EDTA. The aberrant mobility of EF-SAM (~21 kDa) compared to the mass spectrometry-confirmed molecular weight (17.4 kDa) (Stathopoulos et al., 2006) is likely due to localized regions of negative charge (Armstrong and Roman, 1993) and is consistent with the delayed mobility of full-length STIM1 (Baba et al., 2006; Manji et al., 2000). Ca²⁺-loaded Phe108Asp/Gly110Asp was more susceptible to TCA hydrolysis than Ca²⁺-depleted Phe108Asp/Gly110Asp, resulting in greater apparent differences than observed in the size-exclusion chromatography for this mutant (G).

Typical size-exclusion chromatography elution profiles for Ca²⁺-loaded (black lines) and -depleted (red lines) (E) wild-type, (F) P101G, (G) F108D/G110D, (H) F108D/G110D/K113G, (I) A163R, and (J) L195R EF-SAM proteins. Elution buffers were supplemented with 2.5 mM CaCl₂ or 5 mM EDTA. In-line MALS-determined molecular weights were calculated over prominent peaks (circles). Protein was 0.65–0.8 mg ml⁻¹ for each experiment. The void volume is ~8.3 ml in each panel.

behavior of EF-SAM (\pm Ca²⁺), providing a functionally silent control mutation (Figure 3F; Table 1).

EF-SAM coordinates a single Ca²⁺ ion (Stathopoulos et al., 2006) despite the presence of an EF-hand pair. We postulated that Ca²⁺ binding in the hEF2 loop was evolutionarily lost for adaptation to the high Ca²⁺ levels of the lumen. Of the six residues involved in Ca²⁺ coordination, four within STIM hEF2 loops (Z, #, x, and z) appear with >10% frequency in a survey of EF-hand proteins (Figure 2E) (Marsden et al., 1990). However, the first two liganding residues (X and Y), which are highly invariant Asp residues among EF-hand proteins (Marsden et al., 1990), occur

as Phe108 and Gly110, respectively, in STIM1. We prepared a Phe108Asp/Gly110Asp double mutant to increase the Ca²⁺ affinity of EF-SAM via cooperative Ca²⁺ binding between cEF1 and hEF2 (Figure 3A), somewhat analogous to previous CaM studies (Maune et al., 1992; Starovasnik et al., 1992). This double mutant has wild-type-like EF-SAM Ca²⁺ affinity and binding stoichiometry (Figure 4A), but it is constitutively aggregated (Figures 3D and 3G; Table 1); furthermore, the secondary structure persistently (\pm Ca²⁺) resembles Ca²⁺-free wild-type EF-SAM (Figures 4B and 4C). The ability of the double mutant to bind Ca²⁺ in the destabilized state is not surprising given that some residual

Table 1. EF-SAM Mutagenesis Summary

Mutation ^a	Motif	Quaternary Structure ^b	
		+Ca ²⁺	–Ca ²⁺
Wild-type	EF-SAM	Monomer	Dimer/ aggregate
D76A	cEF1 loop	Dimer/ aggregate	Dimer/ aggregate
E87A	cEF1 loop	Aggregate	Aggregate
P101G	hEF2	Monomer	Aggregate
F108D/G110D	hEF2 loop	Dimer/ aggregate	Dimer/ aggregate
F108D/G110D/ K113G	hEF2 loop	Monomer	Dimer/ aggregate
W132R	SAM- α 6-N	Monomer	Dimer/ aggregate
E152R	SAM- α 7	Monomer	Aggregate
A163R	SAM- α 8	Monomer	Dimer/ aggregate
L167R	SAM- α 8	Aggregate	Aggregate
T172R	SAM- α 9	Monomer/ aggregate	Aggregate
L179R	SAM- α 9/ α 10	Monomer	Aggregate
L195R	SAM- α 10	Monomer/ aggregate	Dimer/ aggregate

^a See Experimental Procedures for details regarding mutagenesis rationale.

^b Quaternary structure (\pm Ca²⁺) was assessed by using gel filtration with in-line MALS in which species populating a minimum of 5% of the total λ_{280} UV absorbance were considered significant; structures of a higher order than 2 (dimer) are termed “aggregate.” See Figures 3E–3J for typical results.

structure is retained (Figures 4C and S5C, inset) and even isolated EF-loops preserve metal-binding function (Wojcik et al., 1997). Additionally, the aggregation propensity of this variant is not unexpected given that Phe108 forms part of the hydrophobic cleft for EF-hand:SAM interactions (Figure 2A). Introducing a conserved Gly at position 6 (Phe108Asp/Gly110Asp/Lys113Gly) somewhat rescues Ca²⁺ sensitivity (Figure 3H); however, the decreased stability persists, as Ca²⁺ affinity is greatly reduced with unknown stoichiometry (data not shown). Here, the conformationally flexible Gly may allow for reorganization of the cleft suitable for the EF-hand:SAM intramolecular association at the cost of reduced Ca²⁺ affinity. The hEF2 loop mutations reveal that this motif plays a crucial role in bridging the fold between the EF-hand and SAM domains.

Several modes of SAM domain interaction have been reported previously. A closed dimer is formed via swapping of N-terminal arms with additional interface contacts at the C termini (Stapleton et al., 1999). Another mechanism involves N-terminal arm exchange but leaves the C termini rotated away from each other, forming a second b-interface for polymerization (Thanos et al., 1999). The third mode occurs via two nonpolar surfaces: the mid-loop (centrally located) and the end-helix (C-terminally located) (Kim et al., 2001, 2002). Here, EF-SAM variants were designed in light of those SAM-mediated oligomerization models

of other proteins combined with structure-based sequence alignment (Figures 3A, 3B, and S3). Trp132Arg (loop between α 5 and α 6; N-terminal arm), Glu152Arg (α 7; conserved charge), Ala163Arg (α 8; mid-loop), and Leu179Arg (loop between α 9 and α 10; mid-loop) mutants retain wild-type-like EF-SAM oligomerization properties (Figure 3I; Table 1). However, the SAM hydrophobic core mutant Leu167Arg (α 8; mid loop) and the α 9 helix-destabilizing Thr172Arg (mid-loop) variant are constitutively aggregated (\pm Ca²⁺) (Table 1). Since Ca²⁺ binding to EF-SAM precludes oligomerization (Figures 3C and 3E), the residues buried at the domain interface must play a central role in SAM-mediated associations. As expected, disruption of the EF-hand:SAM intramolecular interaction (Figure 2) with Leu195Arg (α 10; end-helix) results in persistent aggregation (Figure 3J; Table 1). Whereas Leu195 and Leu199 provide the principal hydrophobic anchors to the EF-hand cleft, at least two other α 10 residues (Leu192, Val198) pack against the “open” interface of the EF-hand pair. The collective solvent exposure (upon Ca²⁺-depletion) of all hydrophobic α 10 interface residues likely drives SAM aggregation through the formation of thermodynamically favorable (Figure S5D), intermolecular nonpolar contacts coupled with partial unfolding of the domain (Figures 4B–4D).

Overall, Ca²⁺ binding (cEF1) as well as EF-hand:SAM disruption (hEF2; SAM- α 10) and SAM hydrophobic core mutations can potentiate EF-SAM aggregation in a Ca²⁺-insensitive manner, whereas many variants known to inhibit oligomerization in other SAM domains are incapable of constitutively monomerizing EF-SAM.

Amorphous Structure of Ca²⁺-Depleted and Mutant EF-SAM

Since aggregate polydispersity precludes NMR and X-ray analysis, we employed transmission electron microscopy (TEM) to probe the structure of oligomerized EF-SAM. TEM of Ca²⁺-loaded wild-type EF-SAM (2.5 \times 3.0 nm) was beyond the resolution of the instrument. Consistent with SEC (Figure 3E) and dynamic light scattering (data not shown), a range of aggregate sizes is observed with Ca²⁺-free EF-SAM (\sim 10 to several 100 nm); furthermore, the aggregates appear amorphous in all higher-order assemblies (Figure S4A). TEM was also performed on the Phe108Asp/Gly110Asp mutant EF-SAM. The data show a very similar range of sizes and morphologies for the Ca²⁺-loaded and Ca²⁺-depleted mutant (Figures S4B and S4C) as those observed with the Ca²⁺-depleted wild-type samples. Although it is difficult to resolve specific detail within the partially unfolded EF-SAM aggregates, the present results are in contrast to those for other SAM domains such as TEL, Yan, Scm, and polychrome, which assemble into ordered polymeric filaments, as observed by TEM, involving primarily native-like SAM structure (Qiao and Bowie, 2005). Our results suggest a SAM interaction mechanism dependent on stability and folding of SAM in which the interaction with the neighboring EF-hand domain plays a crucial role; disruption of the EF-hand:SAM interface drives oligomerization coupled with partial unfolding.

Punctae Formation and SOCE Influx in Cells

EF-SAM undergoes substantial destabilization upon Ca²⁺ release (Stathopoulos et al., 2006) concurrent with aggregation,

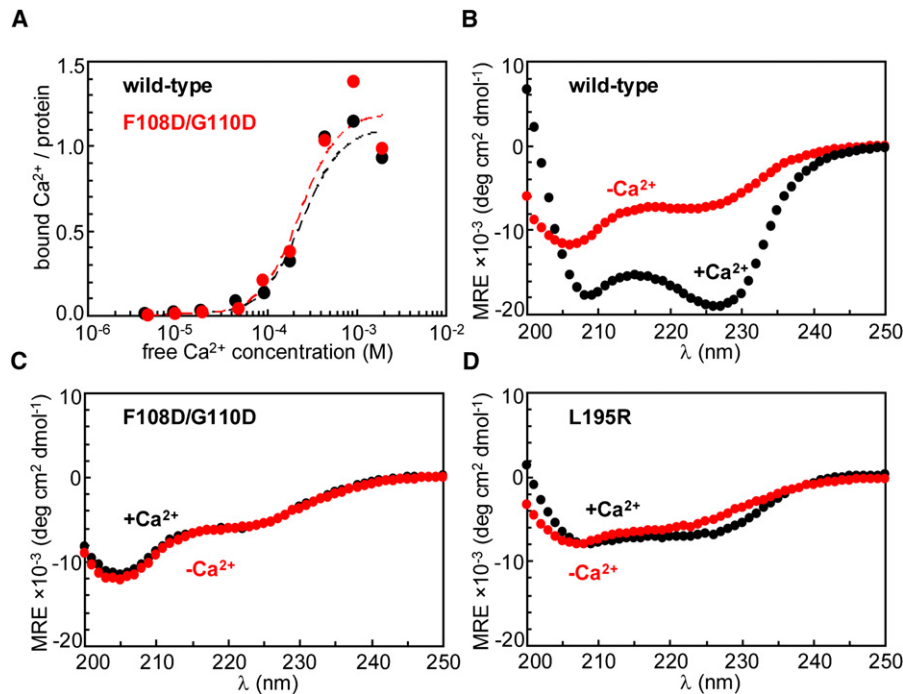


Figure 4. EF-Hand:SAM Interactions Promote a Compact Fold

(A) $^{45}\text{Ca}^{2+}$ binding to wild-type (black circles) and F108D/G110D (red circles) EF-SAM. Each curve was fit to the Hill equation, yielding dissociation constants, $K_D = 248 \pm 68$ and $232 \pm 52 \mu\text{M}$ with stoichiometries of 1.10 ± 0.15 and 1.20 ± 0.14 for wild-type and F108D/G110D, respectively (broken lines). $^{45}\text{Ca}^{2+}$ -binding assays were performed as previously described (Stathopoulos et al., 2006), by using 0.87 mg ml^{-1} protein.

Far-UV CD spectra of (B) wild-type, (C) F108D/G110D, and (D) L195R EF-SAM in the presence (black circles) and absence (red circles) of Ca^{2+} at 20°C . Ca^{2+} -free spectra were acquired in 0.5 mM EDTA buffer, whereas Ca^{2+} -loaded spectra were acquired after the addition of 5 mM CaCl_2 to the Ca^{2+} -free samples. All spectra were normalized as mean residue ellipticity (MRE) based on protein concentration ($0.2\text{--}0.5 \text{ mg ml}^{-1}$).

whereas full-length STIM1 rapidly oligomerizes (Liou et al., 2007) and redistributes into punctae upon luminal Ca^{2+} depletion concomitant with activation of SOC channels (Liou et al., 2005, 2007; Luik et al., 2006; Mercer et al., 2006; Wu et al., 2006; Zhang et al., 2005). These observations taken together with our mutational analysis suggest that EF-SAM stability plays a major role in STIM function. To test this supposition, we engineered Glu87Ala, Phe108Asp/Gly110Asp, and Leu195Arg variants of full-length STIM1, N-terminally tagged with the cherry variant of green fluorescent protein (cherryFP). CherryFP-STIM1 was transiently transfected into HeLa cells, and localization was assessed by using total internal reflective fluorescence (TIRF) microscopy. Wild-type-expressing cells show a diffuse and tubular distribution coexistent with replete Ca^{2+} stores (Figure 5A). This appearance is consistent with previous studies (Baba et al., 2006; Liou et al., 2005; Mercer et al., 2006) in which fibrillar manifestation may be linked with the subcompartmentalization of STIM1 within the ER (Baba et al., 2006). Depletion of the luminal Ca^{2+} stores with thapsigargin results in a redistribution of wild-type to distinct punctae (Figure 5A). The Glu87Ala Ca^{2+} -binding mutation results in constitutive punctae and insensitivity to thapsigargin (Figure 5A), as observed previously (Liou et al., 2005; Mercer et al., 2006; Spassova et al., 2006; Zhang et al., 2005). Similarly, the hEF2 Phe108Asp/Gly110Asp and Leu195Arg destabilization mutants are insensitive to the depletion of ER stores and demonstrate persistent punctae (Figure 5A).

We monitored SOC channel activity by using Fura-2 fluorescence to confirm that punctae formation is linked to SOC channel function. HeLa cells were transiently cotransfected with Orai1 plus cherryFP-STIM1, and the fluorescence response to the addition of external Ca^{2+} or thapsigargin was examined on population monolayers. Upon the addition of thapsigargin to cells bathed in Ca^{2+} -free buffer, the emptying of Ca^{2+} from the ER stores into the cytoplasm is observed as a similar transient increase in the F_{340}/F_{380} ratio for control and mutant transfected cells (Figure 5B). Addition of Ca^{2+} to wild-type-expressing and untreated cells initially bathed in the Ca^{2+} -free medium results in a diminutive increase in the intracellular Ca^{2+} (Figure 5C). However, Glu87Ala, Phe108Asp/Gly110Asp, and Leu195Arg mutants all demonstrate a sustained and marked augmentation of cytoplasmic Ca^{2+} upon extracellular Ca^{2+} addition, consistent with persistently open SOC channels (Figure 5C). Fura-2 fluorescence quenching by SOC channel-permeable Mn^{2+} (Kass et al., 1990) in single-cell experiments was employed to confirm the population data. CherryFP-STIM1 transfected cells were initially bathed in HBSS plus 1.5 mM CaCl_2 or HBSS plus 1.5 mM CaCl_2 and $2 \mu\text{M}$ thapsigargin. Fluorescence quenching was induced with the addition of 2 mM MnCl_2 . Untreated and wild-type STIM1 transfected cells show a marked increase in the quench rates when pretreated with thapsigargin, consistent with thapsigargin-induced activation of SOC channels (Figure 5D). However, cells expressing the mutant proteins

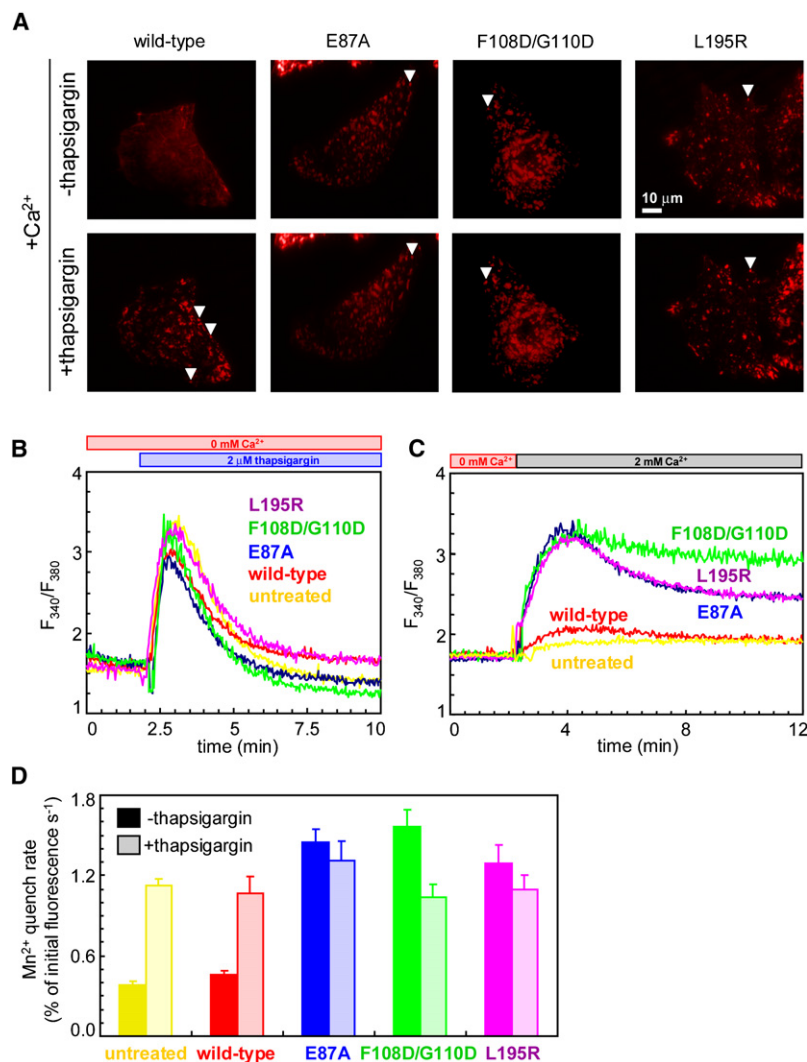


exhibit augmented quench rates constitutively (\pm thapsigargin), similar to the thapsigargin-induced rates observed for the control cells (Figure 5D); these mutant data are coherent with persistently open SOC channels. Both the Fura-2 ratiometric and quench data are in full agreement with the biophysical characterization of the EF-SAM mutants described above, underscoring that stability of the N-terminal Ca^{2+} -sensing region is crucial to STIM1 function.

DISCUSSION

The present EF-SAM structure shows the structural architecture of a luminal EF-hand sensor tailored to the dynamic ER Ca^{2+} signaling range of $\sim 100\text{--}800\ \mu\text{M}$ (Feske, 2007; Hogan and Rao, 2007). The structure unveils a key functional component of STIM proteins with respect to SOCE regulation: a “hidden” EF-hand. This EF-hand does not bind Ca^{2+} , but it is vital for EF-hand:SAM intramolecular association and the mutually linked folding and stability of the EF-SAM entity. Lack of Ca^{2+} coordination to this “hidden” motif contributes to the effectively

Figure 5. EF-SAM Destabilization within Full-Length STIM1 Constitutively Activates SOCE

(A) TIRF microscopy of HeLa cells expressing cherryFP-STIM1. The images show typical HeLa cells expressing wild-type and mutant cherryFP-STIM1 before (upper) and ~ 10 min after (lower) the addition of $2\ \mu\text{M}$ thapsigargin at ambient temperature. A $10\ \mu\text{m}$ scale bar is indicated (upper right).

(B) Relative thapsigargin-evoked transient Ca^{2+} changes of control and cherryFP-STIM1-transfected HeLa cells. Fura-2-loaded cells were bathed in HBSS plus $1\ \text{mM}$ EGTA; $2\ \mu\text{M}$ thapsigargin was subsequently added to the Ca^{2+} -free medium.

(C) Relative Ca^{2+} influx in control and cherryFP-STIM1-transfected HeLa cells. Fura-2-loaded cells were bathed in HBSS plus $1\ \text{mM}$ EGTA; $3\ \text{mM}$ CaCl_2 was subsequently added to the Ca^{2+} -free medium. Cells were cotransfected with Orai1, and experiments were performed on population monolayers in (B) and (C). Results are representative of at least three separate experiments.

(D) Mn^{2+} quenching of Fura-2 fluorescence in control and cherryFP-STIM1-transfected HeLa cells. Fura-2 loaded cells were initially bathed in HBSS plus $1.5\ \text{mM}$ CaCl_2 or HBSS plus $1.5\ \text{mM}$ CaCl_2 and $2\ \mu\text{M}$ thapsigargin. Quenching was induced with the addition of $2\ \text{mM}$ MnCl_2 . Cells expressing STIM1 were identified by cherryFP fluorescence. Each bar is the mean quench rate of at least nine cells from three separate experiments. Error bars represent the standard error of the mean (SEM).

low Ca^{2+} affinity of $\sim 250\ \mu\text{M}$ of this ER-localized domain. The SAM domain as a stability-regulating component within STIM1 is an additional paradigm in an already diverse set of known SAM functions that includes mediating native homo- and heterotypic SAM oligomerization, as well as non-SAM protein, lipid, and RNA binding in transcriptional, translational, and signal transduction roles (Kim and Bowie, 2003; Qiao and Bowie, 2005). Ca^{2+} -depletion of EF-

SAM is functionally coupled with destabilization, which leads to partial unfolding and aggregation, as EF-SAM destabilizing mutations within full-length STIM1 constitutively activate SOCE.

In the absence of NMR or X-ray data, we calculated a hypothetical “closed” Ca^{2+} -depleted EF-SAM model based on the 3D structure of C-terminal apo-CaM (1F71.PDB) to gain insight into the submolecular oligomerization steps. The paired helices of the EF-hand domain adopt a more parallel conformation in the predicted “closed” mode compared to the “open” (Figures S5A and S5B). This conformational change leads to eradication of the hydrophobic cleft, excluding SAM from intimate interaction with the EF-hands. The “closed” model predicts that Val68, Ile71, Leu74, Met75, Leu96, Lys104, Phe108, Ile115, Leu192, Leu195, Val198, and Leu199 (residues at the EF-hand:SAM interface in the “open” Ca^{2+} -loaded state) become solvent exposed (Figure S5B), thereby leading to an unstable state.

Consistent with this hypothesis, our previous studies revealed that depletion of Ca^{2+} from EF-SAM increases the overall hydrophobicity of the protein (Stathopoulos et al., 2006), counter to what is observed for “closed” apo-CaM (Figure S2B) (Yap

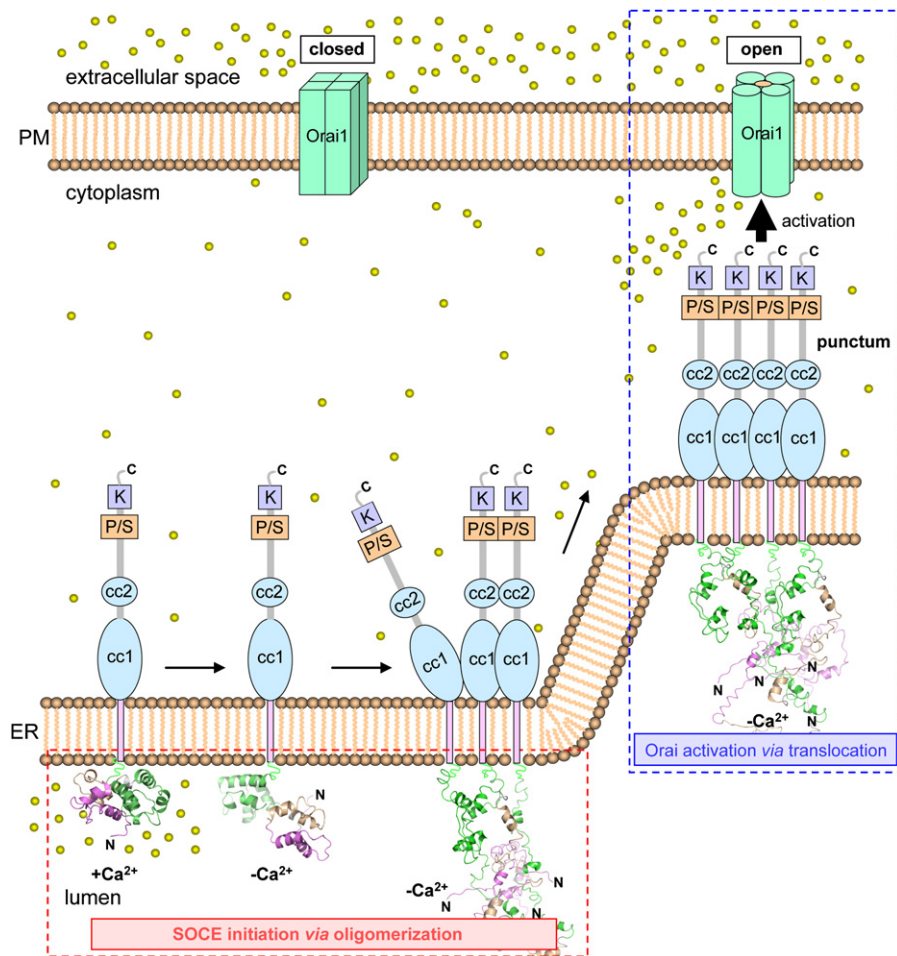


Figure 6. EF-SAM Oligomerization Initiates STIM1 Punctae Formation in the Proposed Orai1 Activation Model of SOCE

With ER stores replete of Ca^{2+} , the luminal portion of STIM1 suppresses homotypic STIM associations via the compact tertiary fold of Ca^{2+} -loaded EF-SAM. This stable fold is promoted by intimate hydrophobic “open” EF-hand:SAM interactions. Ca^{2+} depletion induces a “closed” EF-SAM conformation, exposing several hydrophobic residues on both the EF-hand and SAM domains to solvent. Oligomerization of this unstable EF-SAM conformation is energetically favorable and occurs at the luminal portion of STIM1. This initial EF-SAM oligomerization is presumably augmented by C-terminal, homotypic coiled-coil interactions (Baba et al., 2006; Williams et al., 2002). Oligomers translocate (Liou et al., 2007) into larger assemblies at ER-PM junctions (punctae) (Luik et al., 2006; Wu et al., 2006; Zhang et al., 2005) that trigger SOC channel opening through the C-terminal portion of STIM. Nomenclature is as per Figure 1A.

et al., 1999). Furthermore, the near-UV CD of Ca^{2+} -depleted EF-SAM shows little tertiary structure in the local environment of all aromatics (cEF1 and hEF2: 6 total with 2 Trp; SAM: 6 total with 2 Trp) compared to the compact structure of the Ca^{2+} -loaded state (Figure S5C). Additionally, the deconvoluted far-UV CD-based α helicity is 15% versus 61% for Ca^{2+} -depleted compared to -loaded EF-SAM, respectively (Figure S5C, inset). As the EF-hand region accounts for 25% of the 61% α helicity (NMR structure), the conformational destabilization must proceed through both domains. Together, the data construe an oligomerization mechanism (Figure S5D) by which the “open” Ca^{2+} -loaded EF-SAM is the most stable species in the equilibrium. We believe that the “closed” Ca^{2+} -depleted conformation is destabilized, at least in part, due to exposure of hydrophobics (in cEF1, hEF2, and SAM α 10) and probably exists only transiently. Since the “open” conformation is scarcely accessible in the absence

of Ca^{2+} , “closed” EF-SAM forms oligomers in an energetically downhill mechanism of assembly. The final aggregated EF-SAM state is coupled with partial unfolding of EF-SAM, as evidenced by CD (Figures 4B–4D and S5C). Remarkably, the aggregates can reversibly return to the well-folded monomeric state upon Ca^{2+} binding (Figures 4B and S5C).

Meyer and coworkers (Liou et al., 2007) reported elegant in-cell studies by which they proposed a STIM1-mediated SOCE activation model. The present study further enriches the proposed model by refining the initial phase of the SOCE activation (Figure 6). With replete Ca^{2+} stores, EF-SAM exists as a well-folded monomer and SOC channels are closed; Ca^{2+} depletion induces partial unfolding coupled with oligomerization of EF-SAM. Rapid EF-SAM oligomerization represents the SOCE initiation mechanism and is in agreement with results from full-length STIM1 live-cell experiments identifying this important

preliminary oligomerization phase (Liou et al., 2007). In an appreciably slower event that activates the SOC channel (half-maximal time of ~ 30 – 40 s) (Liou et al., 2007; Wu et al., 2006), oligomers translocate (Liou et al., 2007; Zhang et al., 2005) and assemble into larger aggregates at ER-PM junctions (punctae) in the immediate vicinity of Orai1 (Luik et al., 2006; Wu et al., 2006; Xu et al., 2006; Zhang et al., 2005). The coiled-coil domains of STIM1 mediate constitutive homotypic interactions (Baba et al., 2006; Williams et al., 2002) and must play an important role in the further stabilization of the EF-SAM-triggered oligomers as well as in the translocation to ER-PM junctions. The amorphous nature of EF-SAM aggregates (Figure S4) also suggests an essential role for this cytoplasmic portion of STIM1 in mediating punctae ultrastructure characteristics; hence, an orchestrated structural rearrangement of the entire STIM1 molecule is responsible for channel activation directed through the C-terminal region (Baba et al., 2006; Huang et al., 2006; Liou et al., 2007). At present, it is unclear whether the Orai1 SOC channel is opened via direct (Ong et al., 2007; Vig et al., 2006a; Yeromin et al., 2006) or indirect (Gwack et al., 2007) coupling to STIM1 punctae. In summary, the present study demonstrates the significance of EF-SAM oligomerization in SOCE initiation and provides evidence for its coupling to partial unfolding within this luminal region of STIM molecules. Consistent with the influence of EF-SAM-mediated oligomerization in SOCE initiation, Luik et al. (2008) recently showed that FRB/FKBP oligomerization modules can functionally substitute for EF-SAM, triggering Ca^{2+} -independent punctae formation and Orai1 activation when crosslinked with a rapalog. The cytoplasmic coiled-coil region may contribute to the complexity of the aggregation and activation mechanism of STIM molecules required for Orai channel activation.

Protein instability and partial unfolding associated with aggregation is the basis for numerous protein conformational diseases; however, intrinsically unstructured proteins also have essential nonpathological roles in transcription, translation, posttranslational modification, and the assembly of large protein complexes (Dyson and Wright, 2005). STIM proteins take advantage of this inherent ability as the foundation for SOCE activation. As protein folding and stability represent intrinsic regulatory mechanisms in the function of most, if not all, proteins, the notion of SOC channel regulation by the extrinsic stability of the luminal N-terminal region of STIM proteins is not unfounded. The ER lumen is adapted for such a mechanism with resident molecular chaperones (i.e., heat shock proteins), folding enzymes (protein disulfide isomerases), and stress response (unfolded protein response [UPR]) (Hebert and Molinari, 2007; Ron and Walter, 2007). Furthermore, thapsigargin (i.e., luminal Ca^{2+} depletion) is known to induce ER stress and activate the UPR (Chen et al., 2007), whereas knockdown of STIM1 RNA fails to provoke the UPR in *C. elegans* intestinal cells (Yan et al., 2006). The present molecular mechanistic study on human STIM supports these cellular observations in the worm and prompts speculation regarding the involvement of STIM in Ca^{2+} -depletion-dependent ER stress and UPR activation in other cell types. For example, STIM1 may function as an activator of the UPR due to rapid conversion to the partially unfolded state upon Ca^{2+} depletion. Additionally, UPR upregulation of chaperones may promote faster conversion of punctae back to the “native” monomeric state,

suggestive of an intriguing negative feedback mechanism for SOCE. Further studies are needed to examine these and other potential roles of STIM punctae in ER function.

EXPERIMENTAL PROCEDURES

Protein Expression and Purification

Unlabeled and ^{15}N , ^{13}C -labeled EF-SAM was recombinantly expressed in *E. coli* and was purified under denaturing conditions as previously described (Stathopoulos et al., 2006). All mutagenesis was performed by using the Quik-Change protocol (Stratagene; Agilent Technologies Co.). Ca^{2+} -free proteins were prepared by dialysis versus 25 mM EDTA. Protein concentration was determined by using $\epsilon_{280\text{ nm}} = 1.54$ (mg ml $^{-1}$) cm $^{-1}$. All experiments were performed in 20 mM Tris, 100 mM NaCl (pH 7.5), unless otherwise stated. Ca^{2+} -loaded buffers were supplemented with 2–5 mM CaCl_2 , whereas Ca^{2+} -free buffers contained 5 mM EDTA.

NMR Structure Determination

NMR experiments were performed on 500 and 600 MHz Inova (Varian, Inc.) or 800 and 900 MHz Avance (Bruker Biospin Ltd.) spectrometers equipped with cryogenic, triple-resonance probes. Chemical shifts were assigned by using XEASY (CARA v1.5) after data processing with NMRPipe v2.3. CYANA v2.1 was used for automated structure calculation based on >92% complete chemical shift assignments and ^{15}N -edited and ^{13}C -edited NOESY peak lists. Water refinement of structures was performed in CNS v1.2. See Supplemental Experimental Procedures for further details.

Mutational Rationale

Ca^{2+} -binding knockout mutations were at canonical liganding residues X (D76A) and z (E87A); mutations intended to mobilize binding were at positions X (F108D), Y (G110D), and position 6 of the “hidden” loop (K113G) rationalized from sequence alignments (Figure 2E). SAM mutations intended to alleviate aggregation (W132R, E152R, A163R, L167R, T172R, L179R) were inferred from structure-based alignments with other SAM domains (Figure S3). See Supplemental Experimental Procedures for further details.

Size-Exclusion Chromatography

Size-exclusion chromatography (SEC) was performed on Superdex S200 10/300 GL columns by using an AKTA FPLC system (GE Healthcare Life Sciences) at 4°C.

Light Scattering

MALS measurements were done in-line with SEC by using a three-angle (45°, 90°, and 135°) miniDawn light-scattering instrument equipped with a 690 nm laser and an Optilab rEX differential refractometer (Wyatt Technologies, Inc.). Molecular weight was calculated by using the ASTRA software (Wyatt Technologies, Inc.) based on Zimm plot analysis and by using a protein refractive index increment, $dn\ dc^{-1} = 0.185$ L g $^{-1}$.

Circular Dichroism

Data were acquired on a Jasco J-815 CD Spectrometer (Jasco, Inc.). For far-UV CD spectra, data were collected in 1 nm increments (20 nm/min) by using 0.01 or 0.1 cm pathlength cuvettes, a 8 s averaging time, and 1 nm bandwidth. Near-UV CD spectra were collected in 0.5 cm pathlength cuvettes by using the same parameters. Spectra were corrected for buffer contributions.

Transmission Electron Microscopy

Protein solutions at 0.2 mg ml $^{-1}$ were incubated on 400-mesh formvar copper grids (Electron Microscopy Sciences, Inc.) for 1 min. After blotting off the solution with 3MM CHR Whatman filter paper (Whatman, Inc.), the grids were air dried for 1 min. Subsequently, 2% w/v uranyl acetate was applied and immediately blotted off. Specimens were viewed with a FEI Tecnai 20 transmission electron microscope (FEI Co.) at an accelerating voltage of 200 keV. Images were digitized with a Gatan Dualview CCD camera (Gatan, Inc.).

Mammalian Cell Culture and Transfection

HeLa cells were cultured in Dulbecco's modified Eagle's medium (HyClone Thermo Fisher Scientific, Inc.) supplemented with 5%–10% v/v fetal bovine serum (GIBCO-BRL, Inc.), 100 U ml⁻¹ penicillin, and 100 µg ml⁻¹ streptomycin (Sigma-Aldrich Co.). Cells were maintained in a 95% air, 5% CO₂ environment at 37°C. Full-length cherryFP-STIM1 was in the pCMV6-XL5 vector, obtained as a gift from R.S. Lewis (Stanford University) (Luik et al., 2006). Full-length Orai1 was in the pCMV6-XL5 vector and was purchased from Origene (Origene Technologies, Inc.). For fluorescence microscopy, cells were cultured on 35 mm (No 0) glass-bottom plates (MarTek Corp.), and for fluorescence spectroscopy experiments, cells were cultured on rectangular, glass coverslips to 50%–80% confluence. Transfection was performed with Lipofectamine LTX or Lipofectamine 2000 (Invitrogen, Inc.).

Fluorescence Microscopy

Growth medium was exchanged for nominally Ca²⁺-free HEPES-buffered saline solution (HBSS); 20 mM HEPES, 120 mM NaCl, 5.4 mM KCl, 0.8 mM MgSO₄, 10 mM D-glucose [pH 7.4]) prior to imaging. Fluorescence images were acquired on an Olympus IX70 (Olympus, Inc.) inverted microscope with a 60× oil-immersion TIRF objective (N.A. 1.45) (Olympus, Inc.), illuminated by a 543.5 nm HeNe laser (05-LGP-193; 5 mW) (Melles Griot Laser Group) for cherryFP or by a Xenon light (125 W; λ_{ex} ~360 nm) for Fura-2 imaging. Excitation light was reflected by a 485-555-650TBDR dichroic, and emitted light was passed through a 515-600-730TBEM filter (Omega Optical, Inc.). Images were digitized with a cooled Evolution QEI CCD camera (Media Cybernetics, Inc.).

Fura-2 Fluorescence Experiments

Cells were intracellularly loaded with the addition of 2 µM Fura-2-acetoxymethyl ester (Sigma-Aldrich Co.) to the growth medium and incubation at ambient temperature for 30 min in the dark. Fluorescence emission (λ_{em} = 490 nm; slit = 10 nm) with λ_{ex} = 340 and 380 nm (slit = 3 nm) was measured with a Shimadzu RF-5301PC fluorimeter (Shimadzu Corp.). Experiments were performed on population monolayers after washing and appropriately orienting the coverslip in a 4 ml (1 cm pathlength) quartz cuvette filled with HBSS plus 1 mM EGTA. Experiments were commenced after a 3 min equilibration. Data were collected every 2 s with the addition of 3 mM CaCl₂ or 2 µM thapsigargin (Sigma-Aldrich Co.) to the HBSS. Background fluorescence at F₃₄₀ and F₃₈₀ was subtracted prior to F₃₄₀/F₃₈₀ calculation. The R_{max} was estimated at ~10. For Mn²⁺ quench experiments, cells were bathed in HBSS (+1.5 mM CaCl₂) and equilibrated with or without 2 µM thapsigargin. Images were acquired before and after the addition of 2 mM MnCl₂ every 2.5 s as described in the "Fluorescence Microscopy" section. The change in fluorescence for each image was normalized to the resting fluorescence (ΔF/F) of each cell prior to the determination of quench rates by linear regression. See [Supplemental Experimental Procedures](#) for further details.

Bioinformatics and Modeling Programs

Alignments were done with Dali, DaliLite, and CLUSTAL W. Molecular images were rendered with PyMOL and MOLMOL. The "closed" EF-SAM model was calculated with Modeler. See [Supplemental Experimental Procedures](#) for further details.

ACCESSION NUMBERS

Atomic coordinates have been deposited in the Protein Data Bank under accession code 2k60 (rcsb100719); all constraints and chemical shifts have been deposited in the Biological Magnetic Resonance Bank under accession code 15851.

SUPPLEMENTAL DATA

Supplemental Data include Supplemental Experimental Procedures, five figures, and two tables and are available with this article online at <http://www.cell.com/cgi/content/full/135/1/110/DC1/>.

ACKNOWLEDGMENTS

We thank N. Ishiyama for his EM assistance, R.S. Lewis (Stanford University) for providing cherryFP-STIM1, and Bruker Biospin Corporation (Fremont, CA) for 900 MHz NMR time. This research was made possible through a Canadian Institutes of Health Research operating grant, a Canadian Foundation for Innovation grant for an 800 MHz NMR spectrometer, and Natural Sciences and Engineering Research Council of Canada and Ontario Cancer Institute Knudson fellowships (to P.B.S.). M.I. holds the Canada Research Chair in Cancer Structural Biology.

Received: March 10, 2008

Revised: May 26, 2008

Accepted: August 1, 2008

Published: October 2, 2008

REFERENCES

- Armstrong, D.J., and Roman, A. (1993). The anomalous electrophoretic behavior of the human papillomavirus type 16 E7 protein is due to the high content of acidic amino acid residues. *Biochem. Biophys. Res. Commun.* **192**, 1380–1387.
- Baba, Y., Hayashi, K., Fujii, Y., Mizushima, A., Watarai, H., Wakamori, M., Numaga, T., Mori, Y., Iino, M., Hikida, M., and Kurosaki, T. (2006). Coupling of STIM1 to store-operated Ca²⁺ entry through its constitutive and inducible movement in the endoplasmic reticulum. *Proc. Natl. Acad. Sci. USA* **103**, 16704–16709.
- Berridge, M.J., Bootman, M.D., and Roderick, H.L. (2003). Calcium signaling: dynamics, homeostasis and remodelling. *Nat. Rev. Mol. Cell Biol.* **4**, 517–529.
- Cai, X. (2007). Molecular evolution and functional divergence of the Ca²⁺ sensor protein in store-operated Ca²⁺ entry: stromal interaction molecule. *PLoS ONE* **2**, e609.
- Chen, L.H., Jiang, C.C., Kiejda, K.A., Wang, Y.F., Thorne, R.F., Zhang, X.D., and Hersey, P. (2007). Thapsigargin sensitizes human melanoma cells to TRAIL-induced apoptosis by up-regulation of TRAIL-R2 through the unfolded protein response. *Carcinogenesis* **28**, 2328–2336.
- Chin, D., and Means, A.R. (2000). Calmodulin: a prototypical calcium sensor. *Trends Cell Biol.* **10**, 322–328.
- Dyson, H.J., and Wright, P.E. (2005). Intrinsically unstructured proteins and their functions. *Nat. Rev. Mol. Cell Biol.* **6**, 197–208.
- Feske, S. (2007). Calcium signalling in lymphocyte activation and disease. *Nat. Rev. Immunol.* **7**, 690–702. Published online August 17, 2007. 10.1038/nri2152.
- Feske, S., Gwack, Y., Prakriya, M., Srikanth, S., Puppel, S.H., Tanasa, B., Hogan, P.G., Lewis, R.S., Daly, M., and Rao, A. (2006). A mutation in Orai1 causes immune deficiency by abrogating CRAC channel function. *Nature* **441**, 179–185.
- Gwack, Y., Srikanth, S., Feske, S., Cruz-Guilloty, F., Oh-hora, M., Neems, D.S., Hogan, P.G., and Rao, A. (2007). Biochemical and functional characterization of Orai proteins. *J. Biol. Chem.* **282**, 16232–16243.
- Hebert, D.N., and Molinari, M. (2007). In and out of the ER: protein folding, quality control, degradation, and related human diseases. *Physiol. Rev.* **87**, 1377–1408.
- Hogan, P.G., and Rao, A. (2007). Dissecting ICRAC, a store-operated calcium current. *Trends Biochem. Sci.* **32**, 235–245.
- Huang, G.N., Zeng, W., Kim, J.Y., Yuan, J.P., Han, L., Muallem, S., and Worley, P.F. (2006). STIM1 carboxyl-terminus activates native SOC, I(crac) and TRPC1 channels. *Nat. Cell Biol.* **8**, 1003–1010.
- Ikura, M., Minowa, O., and Hikichi, K. (1985). Hydrogen bonding in the carboxyl-terminal half-fragment 78–148 of calmodulin as studied by two-dimensional nuclear magnetic resonance. *Biochemistry* **24**, 4264–4269.

- Ikura, M., Clore, G.M., Gronenborn, A.M., Zhu, G., Klee, C.B., and Bax, A. (1992). Solution structure of a calmodulin-target peptide complex by multidimensional NMR. *Science* 256, 632–638.
- Kanelis, V., Forman-Kay, J.D., and Kay, L.E. (2001). Multidimensional NMR methods for protein structure determination. *IUBMB Life* 52, 291–302.
- Kass, G.E., Llopis, J., Chow, S.C., Duddy, S.K., and Orrenius, S. (1990). Receptor-operated calcium influx in rat hepatocytes. Identification and characterization using manganese. *J. Biol. Chem.* 265, 17486–17492.
- Kim, C.A., and Bowie, J.U. (2003). SAM domains: uniform structure, diversity of function. *Trends Biochem. Sci.* 28, 625–628.
- Kim, C.A., Phillips, M.L., Kim, W., Gingery, M., Tran, H.H., Robinson, M.A., Faham, S., and Bowie, J.U. (2001). Polymerization of the SAM domain of TEL in leukemogenesis and transcriptional repression. *EMBO J.* 20, 4173–4182.
- Kim, C.A., Gingery, M., Pilpa, R.M., and Bowie, J.U. (2002). The SAM domain of polyhomeotic forms a helical polymer. *Nat. Struct. Biol.* 9, 453–457.
- Kretsinger, R.H., and Nockolds, C.E. (1973). Carp muscle calcium-binding protein. II. Structure determination and general description. *J. Biol. Chem.* 248, 3313–3326.
- Liou, J., Kim, M.L., Heo, W.D., Jones, J.T., Myers, J.W., Ferrell, J.E., Jr., and Meyer, T. (2005). STIM is a Ca^{2+} sensor essential for Ca^{2+} -store-depletion-triggered Ca^{2+} influx. *Curr. Biol.* 15, 1235–1241.
- Liou, J., Fivaz, M., Inoue, T., and Meyer, T. (2007). Live-cell imaging reveals sequential oligomerization and local plasma membrane targeting of stromal interaction molecule 1 after Ca^{2+} store depletion. *Proc. Natl. Acad. Sci. USA* 104, 9301–9306.
- Luik, R.M., Wu, M.M., Buchanan, J., and Lewis, R.S. (2006). The elementary unit of store-operated Ca^{2+} entry: local activation of CRAC channels by STIM1 at ER-plasma membrane junctions. *J. Cell Biol.* 174, 815–825.
- Luik, R.M., Wang, B., Prakriya, M., Wu, M.M., and Lewis, R.S. (2008). Oligomerization of STIM1 couples ER calcium depletion to CRAC channel activation. *Nature* 454, 538–542.
- Manji, S.S., Parker, N.J., Williams, R.T., van Stekelenburg, L., Pearson, R.B., Dziadek, M., and Smith, P.J. (2000). STIM1: a novel phosphoprotein located at the cell surface. *Biochim. Biophys. Acta* 1481, 147–155.
- Marsden, B.J., Shaw, G.S., and Sykes, B.D. (1990). Calcium binding proteins. Elucidating the contributions to calcium affinity from an analysis of species variants and peptide fragments. *Biochem. Cell Biol.* 68, 587–601.
- Maune, J.F., Klee, C.B., and Beckingham, K. (1992). Ca^{2+} binding and conformational change in two series of point mutations to the individual Ca^{2+} -binding sites of calmodulin. *J. Biol. Chem.* 267, 5286–5295.
- Meador, W.E., Means, A.R., and Quijoch, F.A. (1993). Modulation of calmodulin plasticity in molecular recognition on the basis of x-ray structures. *Science* 262, 1718–1721.
- Mercer, J.C., Dehaven, W.I., Smyth, J.T., Wedel, B., Boyles, R.R., Bird, G.S., and Putney, J.W., Jr. (2006). Large store-operated calcium-selective currents due to co-expression of Orai1 or Orai2 with the intracellular calcium sensor, Stim1. *J. Biol. Chem.* 281, 24979–24990.
- Ong, H.L., Cheng, K.T., Liu, X., Bandyopadhyay, B.C., Paria, B.C., Soboloff, J., Pani, B., Gwack, Y., Srikanth, S., Singh, B.B., et al. (2007). Dynamic assembly of TRPC1-STIM1-Orai1 ternary complex is involved in store-operated calcium influx. Evidence for similarities in store-operated and calcium release-activated calcium channel components. *J. Biol. Chem.* 282, 9105–9116.
- Peinelt, C., Vig, M., Koomoa, D.L., Beck, A., Nadler, M.J., Koblan-Huberson, M., Lis, A., Fleig, A., Penner, R., and Kinet, J.P. (2006). Amplification of CRAC current by STIM1 and CRACM1 (Orai1). *Nat. Cell Biol.* 8, 771–773.
- Prakriya, M., Feske, S., Gwack, Y., Srikanth, S., Rao, A., and Hogan, P.G. (2006). Orai1 is an essential pore subunit of the CRAC channel. *Nature* 443, 230–233.
- Putney, J.W., Jr. (1986). A model for receptor-regulated calcium entry. *Cell Calcium* 7, 1–12.
- Qiao, F., and Bowie, J.U. (2005). The many faces of SAM. *Sci. STKE* 2005, re7.
- Ron, D., and Walter, P. (2007). Signal integration in the endoplasmic reticulum unfolded protein response. *Nat. Rev. Mol. Cell Biol.* 8, 519–529.
- Roos, J., DiGregorio, P.J., Yeromin, A.V., Ohlsen, K., Lioudyno, M., Zhang, S., Safrina, O., Kozak, J.A., Wagner, S.L., Cahalan, M.D., et al. (2005). STIM1, an essential and conserved component of store-operated Ca^{2+} channel function. *J. Cell Biol.* 169, 435–445. Published online May 2, 2005. 10.1083/jcb.200502019.
- Soboloff, J., Spassova, M.A., Hewavitharana, T., He, L.P., Xu, W., Johnstone, L.S., Dziadek, M.A., and Gill, D.L. (2006a). STIM2 is an inhibitor of STIM1-mediated store-operated Ca^{2+} entry. *Curr. Biol.* 16, 1465–1470.
- Soboloff, J., Spassova, M.A., Tang, X.D., Hewavitharana, T., Xu, W., and Gill, D.L. (2006b). Orai1 and STIM reconstitute store-operated calcium channel function. *J. Biol. Chem.* 281, 9.
- Spassova, M.A., Soboloff, J., He, L.P., Xu, W., Dziadek, M.A., and Gill, D.L. (2006). STIM1 has a plasma membrane role in the activation of store-operated Ca^{2+} channels. *Proc. Natl. Acad. Sci. USA* 103, 4040–4045. Published online March 6, 2006. 10.1073/pnas.0510050103.
- Stapleton, D., Balan, I., Pawson, T., and Sicheri, F. (1999). The crystal structure of an Eph receptor SAM domain reveals a mechanism for modular dimerization. *Nat. Struct. Biol.* 6, 44–49.
- Starovasnik, M.A., Su, D.R., Beckingham, K., and Kleivit, R.E. (1992). A series of point mutations reveal interactions between the calcium-binding sites of calmodulin. *Protein Sci.* 1, 245–253.
- Stathopoulos, P.B., Li, G.Y., Plevin, M.J., Ames, J.B., and Ikura, M. (2006). Stored Ca^{2+} depletion-induced oligomerization of stromal interaction molecule 1 (STIM1) via the EF-SAM region: an initiation mechanism for capacitive Ca^{2+} entry. *J. Biol. Chem.* 281, 35855–35862.
- Strange, K., Yan, X., Lorin-Nebel, C., and Xing, J. (2007). Physiological roles of STIM1 and Orai1 homologs and CRAC channels in the genetic model organism *Caenorhabditis elegans*. *Cell Calcium* 42, 193–203.
- Thanos, C.D., Goodwill, K.E., and Bowie, J.U. (1999). Oligomeric structure of the human EphB2 receptor SAM domain. *Science* 283, 833–836.
- Vig, M., Beck, A., Billingsley, J.M., Lis, A., Parvez, S., Peinelt, C., Koomoa, D.L., Soboloff, J., Gill, D.L., Fleig, A., et al. (2006a). CRACM1 multimers form the ion-selective pore of the CRAC channel. *Curr. Biol.* 16, 2073–2079.
- Vig, M., Peinelt, C., Beck, A., Koomoa, D.L., Rabah, D., Koblan-Huberson, M., Kraft, S., Turner, H., Fleig, A., Penner, R., and Kinet, J.P. (2006b). CRACM1 is a plasma membrane protein essential for store-operated Ca^{2+} entry. *Science* 312, 1220–1223. Published online April 27, 2006. 10.1126/science.1127883.
- Williams, R.T., Manji, S.S., Parker, N.J., Hancock, M.S., Van Stekelenburg, L., Eid, J.P., Senior, P.V., Kazenwadel, J.S., Shandala, T., Saint, R., et al. (2001). Identification and characterization of the STIM (stromal interaction molecule) gene family: coding for a novel class of transmembrane proteins. *Biochem. J.* 357, 673–685.
- Williams, R.T., Senior, P.V., Van Stekelenburg, L., Layton, J.E., Smith, P.J., and Dziadek, M.A. (2002). Stromal interaction molecule 1 (STIM1), a transmembrane protein with growth suppressor activity, contains an extracellular SAM domain modified by N-linked glycosylation. *Biochim. Biophys. Acta* 1596, 131–137.
- Wojcik, J., Goral, J., Pawlowski, K., and Bierzynski, A. (1997). Isolated calcium-binding loops of EF-hand proteins can dimerize to form a native-like structure. *Biochemistry* 36, 680–687.
- Wu, M.M., Buchanan, J., Luik, R.M., and Lewis, R.S. (2006). Ca^{2+} store depletion causes STIM1 to accumulate in ER regions closely associated with the plasma membrane. *J. Cell Biol.* 174, 803–813.
- Xu, P., Lu, J., Li, Z., Yu, X., Chen, L., and Xu, T. (2006). Aggregation of STIM1 underneath the plasma membrane induces clustering of Orai1. *Biochem. Biophys. Res. Commun.* 350, 969–976.
- Yan, X., Xing, J., Lorin-Nebel, C., Estevez, A.Y., Nehrke, K., Lamitina, T., and Strange, K. (2006). Function of a STIM1 homologue in *C. elegans*: evidence that store-operated Ca^{2+} entry is not essential for oscillatory Ca^{2+} signaling and ER Ca^{2+} homeostasis. *J. Gen. Physiol.* 128, 443–459.

Yap, K.L., Ames, J.B., Swindells, M.B., and Ikura, M. (1999). Diversity of conformational states and changes within the EF-hand protein superfamily. *Proteins* 37, 499–507.

Yeromin, A.V., Zhang, S.L., Jiang, W., Yu, Y., Safrina, O., and Cahalan, M.D. (2006). Molecular identification of the CRAC channel by altered ion selectivity in a mutant of Orai. *Nature* 443, 226–229.

Zhang, S.L., Yu, Y., Roos, J., Kozak, J.A., Deerinck, T.J., Ellisman, M.H., Stauderman, K.A., and Cahalan, M.D. (2005). STIM1 is a Ca^{2+} sensor that activates

CRAC channels and migrates from the Ca^{2+} store to the plasma membrane. *Nature* 437, 902–905.

Zhang, S.L., Yeromin, A.V., Zhang, X.H., Yu, Y., Safrina, O., Penna, A., Roos, J., Stauderman, K.A., and Cahalan, M.D. (2006). Genome-wide RNAi screen of Ca^{2+} influx identifies genes that regulate Ca^{2+} release-activated Ca^{2+} channel activity. *Proc. Natl. Acad. Sci. USA* 103, 9357–9362. Published online June 2, 2006. 10.1073/pnas.0603161103.